Ferromagnetic Nitrides with the Filled β-Mn Structure: $Fe_{2-x}M_xMo_3N$ (M = Ni, Pd, Pt)

Timothy J. Prior, Sophie E. Oldham, Victoria J. Couper, and Peter D. Battle*

Inorganic Chemistry Laboratory, Oxford University, South Parks Road, Oxford, OX1 3QR, U.K.

Received December 8, 2004. Revised Manuscript Received January 27, 2005

The introduction of group 10 metals into the hypothetical composition Fe_2Mo_3N allows the isolation of the solid solutions $Fe_{2-x}M_xMo_3N$ (M = Ni, Pd, Pt), which crystallize with the filled β-manganese structure (space group $P4_132$, $a \approx 6.7$ Å). These materials display ferromagnetism with the Curie temperature and saturation magnetization being dependent on the iron content; $Fe_{1.25}M_{0.75}Mo_3N$ shows the highest ordering temperature in each series (maximized at $T_c = 225$ K for M = Pt) and the highest magnetization is always observed for $x = 0.5$ (maximized at 2.44 μ_B per formula unit for M = Pd).

Introduction

The search for new electronic materials remains one of the major driving forces in contemporary solid state chemistry. Metal nitrides are emerging in this area as a class of compounds which frequently displays structures and properties which differ from those of the better-known and more widely studied oxides. They are technologically and academically interesting because of their hardness,[1,2] thermal[3] and electrical[4,5] conductivity, superconductivity,[6] and magnetism,[7] and they find wide-ranging applications in the electronics industry. Small changes in structure or composition lead to significant changes in electrical behavior; for example, the change from metal to insulating behavior of the rock-salt structured TaN_x can be achieved by varying the heating regime and nitrogen pressure during synthesis,[8,9] ZrN_x displays a metal−insulator phase change at $x = 1.33$,[10] and GaN becomes metallic under pressure.[11] Ternary and higher mixed-metal nitrides[12,13] have diverse structures and offer greater scope for control of physical properties through control of electron concentration.

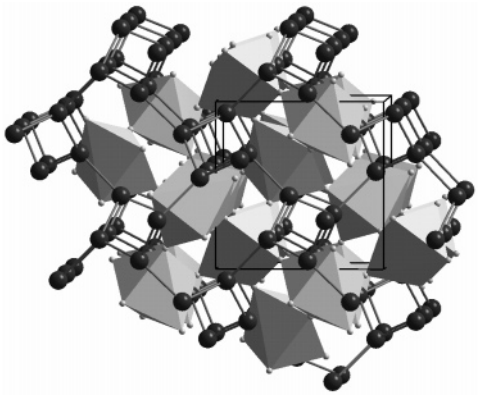

Figure 1. The filled β-Mn structure, M_2T_3X. Space within the (10,3)-a network of M atoms (black) is filled by corner-sharing T_6X octahedra (gray).

The synthesis of mixed-metal nitrides containing d-block elements has frequently involved the use of precursor materials which require rather laborious preparation,[14,15] while the range of products accessible is limited by the stoichiometry of available precursors. We have shown that the synthesis of interstitial mixed-metal nitrides may be greatly simplified: our method employs reduction−nitridation[16] of stoichiometric mixtures of commercially available binary oxides under dilute hydrogen in nitrogen. This method gives access to a wide range of compositions with the filled β-manganese structure and the η-carbide structure.[16,17]

The filled β-manganese structure, M_2T_3X, illustrated in Figure 1, is commonly adopted by interstitial mixed-metal compounds (X = boron, carbon, nitrogen).[18−20] M atoms lie on the 8c positions of cubic unit cell with space group

* To whom correspondence should be addressed. E-mail: peter.battle@chem.ox.ac.uk.

(1) Buhl, R.; Pulker, H. K.; Moll, E. *Thin Solid Films* **1981**, *80*, 265−270.
(2) Oyama, S. T. *The Chemistry of Transition Metal Carbides and Nitrides*; Blackie Academic and Professional: London, 1996.
(3) Watari, K. *J. Ceram. Soc. Jpn.* **2001**, *109*, S7−S16.
(4) Yoshida, S.; Shirakawa, T.; Aritoma, A. In *Proceedings 32nd Electronic Components Conference*; IEEE: New York, 1982; pp 530−535.
(5) Fix, R. M.; Gordon, R. G.; Hoffman, D. M. *Chem. Mater.* **1990**, *2*, 235−241.
(6) Horn, F. H.; Zieglar, W. T. *J. Am. Chem. Soc.* **1947**, *69*, 2762−2769.
(7) Coey, J. M. D.; Smith, P. A. I. *J. Magn. Magn. Mater.* **1999**, *200*, 405−424.
(8) Lu, Y. M.; Weng, R. J.; Hwang, W. S.; Yang, Y. S. *Thin Solid Films* **2001**, *398*, 356−360.
(9) Kaul, A. B.; Whiteley, S. R.; Van Duzer, T.; Yu, L.; Newman, N.; Rowell, J. M. *Appl. Phys. Lett.* **2001**, *78*, 99−101.
(10) Prieto, P.; Galan, L.; Sanz, J. M. *Phys. Rev. B* **1993**, *47*, 1613−1615.
(11) Perlin, P.; Knap, W.; Camassel, J.; Polian, A.; Chervin, J. C.; Suski, T.; Grzegory, I.; Porowski, S. *Phys. Status Solidi B* **1996**, *198*, 223−233.
(12) Gregory, D. H. *J. Chem. Soc.-Dalton Trans.* **1999**, 259−270.
(13) DiSalvo, F. J. *Mater. Sci. Forum* **2000**, *325−6*, 3−10.
(14) Weil, K. S.; Kumta, P. N.; Grins, J. *J. Solid State Chem.* **1999**, *146*, 22−35.
(15) Alconchel, S.; Sapina, F.; Beltran, D.; Beltran, A. *J. Mater. Chem.* **1999**, *9*, 749−755.
(16) Prior, T. J.; Battle, P. D. *J. Solid State Chem.* **2003**, *172*, 138−147.
(17) Prior, T. J.; Battle, P. D. *J. Mater. Chem.* **2004**, *14*, 3001−3007.
(18) Eibenstein, U.; Jung, W. *J. Solid State Chem.* **1997**, *133*, 21−24.
(19) Jeitschko, W.; Nowotny, H.; Benesovsky, F. *Monatsh. Chem.* **1963**, *94*, 247−251.
(20) Jeitschko, W.; Nowotny, H.; Benesovsky, F. *Monatsh. Chem.* **1964**, *95*, 1212−1218.

10.1021/cm047859q CCC: $30.25
Published on Web 03/09/2005

symmetry $P4_132$ forming a single (10,3)-a network.[21] T_6X octahedra share corners to fill the space within this network.

We have previously reported the structure and magnetism of $Fe_{1.5}Pd_{0.5}Mo_3N$, the first filled β-manganese phase to display ferromagnetism.[22] Here we present a full description of the synthesis of the filled β-manganese phases $Fe_{2-x}M_xMo_3N$ (M = Ni, Pd, Pt; $0.5 < x < 2$) and the characterization of their electrical and magnetic properties. This allows us to compare the electronic properties of compounds adopting this structure when the 8c site is partially occupied by elements having 3d, 4d, or 5d valence orbitals, with consequent changes in atomic size and the degree of electron delocalization.

Experimental Details

Synthesis. Polycrystalline samples of $Fe_{2-x}M_xMo_3N$ (M = Ni, Pd, Pt) were prepared by standard ceramic techniques. Stoichiometric mixtures of the appropriate binary metal oxides were intimately ground, pelletized, and fired under a flow of 10% H_2 in N_2 gas (ca. 4.2 $dm^3\ h^{-1}$) for 48 h at 700 °C, 24 h at 750 and 875 °C, and twice at 975 °C, with intermittent regrinding. All reactions were carried out using the above procedure except those involving Pt, when the reaction mixtures were first heated at 500 °C in air for 30 min as loose powders to effect initial decomposition of PtO_2 to PtO_{1+x}. (Reagent purities: iron oxide (Alfa Aesar) 99.998%, molybdenum trioxide (Alfa Aesar) 99.9995%, nickel oxide (Johnson Matthey) 99.95%, palladium oxide (Johnson Matthey) 99.9%, and platinum dioxide (Alfa Aesar) 99.9%. Synthesis gas: 10% H_2 in N_2 (Air Products).)

In all cases furnaces were purged with the synthesis gas prior to heating and samples were cooled to room temperature under gas flow by switching the furnace off. No study of the effects of variation of cooling rate was carried out. No special handling techniques were applied to samples following their removal from the furnace.

Characterization. The progress of each synthesis was charted by X-ray powder diffraction using a Philips PW1750 diffractometer operating with Cu Kα radiation. Relatively high resolution data to be used in quantitative analyses were collected using a Siemens D5000 diffractometer nominally operating with Cu $K\alpha_1$ radiation over the angular range $10 \le 2\theta/° \le 125$ with a step size of $\Delta 2\theta = 0.02°$. However, imperfect monochromation introduced a contribution of approximately 2% $K\alpha_2$ which was allowed for in the data analysis.

Neutron powder diffraction data were collected from ca. 4.6 g of polycrystalline samples of selected compositions using the instruments D1b and D2b, at the Institut Laue Langevin, Grenoble, France. D1b is a high-flux, medium-resolution instrument operating with a mean wavelength of 2.5219 Å. Data were collected over an angular range $18° \le 2\theta \le 98°$ with a step size $\Delta 2\theta = 0.2°$. Samples were contained within vanadium cans which were mounted in a He cryostat during data collection. Scattering attributable to the cans occurs at $2\theta \approx 72°$ and data in this region were excluded from the analysis. D2b is a medium-flux, high-resolution diffractometer which was employed with a mean wavelength of 1.594 Å. Useful data were collected over an angular range $15° \le 2\theta \le 150°$, with a step size $\Delta 2\theta = 0.05°$. Samples were loaded inside vanadium cans for data collection. Rietveld refinement[23] of the crystal structures was carried out using the GSAS[24] and FULLPROF[25,26] suites of programs. Backgrounds were fitted using a shifted Chebyshev polynomial of the first kind. Peak shapes were modeled using a pseudo-Voigt function. Unit cell parameters and atom positions were refined for all samples. An isotropic displacement parameter was initially refined for each atom. In analyses of X-ray data where these values became negative they were set to zero and not refined; this problem did not arise in the analysis of neutron diffraction data.

Magnetic measurements were carried out using a Quantum Design MPMS 5000 SQUID magnetometer. The sample magnetization (M) was measured as a function of temperature ($5 \le T/K \le 300$) during warm up after cooling to 5 K in either zero field (ZFC) or in the measuring field of 100 Oe (FC). In selected cases, the magnetization was measured as a function of field ($-50 \le H/kOe \le 50$) after cooling to the measuring temperature in a field of 50 kOe.

Four-probe conductivity measurements were performed using an apparatus constructed within the laboratory. Bars were cut from pellets which were sintered at 800 °C under the synthesis gas. Contacts were attached using silver paint. Conductivity was measured as a function of temperature in the range $30 \le T/K \le 298$.

Nitrogen analysis was performed by the analytical service of the Inorganic Chemistry Laboratory, Oxford, using a Carlo Erber 1106 CHN analyzer.

Results

Structure Analyses. Seven compositions in the series $Fe_{2-x}Ni_xMo_3N$ were obtained by reduction−nitridation of binary metal oxide mixtures. Analysis of X-ray powder diffraction data showed that a β-manganese phase was always the dominant reaction product and that the unit cell parameter varied inversely with the Ni content. Good fits to the data were obtained using models with disordered Fe and Ni occupying the 8c positions and Mo (12d site) forming Mo_6N octahedra with the interstitial nitrogen atom on the 4a site. Crystal data for these compounds derived from X-ray data are contained in Table 1. Chemical analysis of the nitrogen content, shown in Table 3, suggested full occupancy of the 4a interstitial site in each case. For the compositions $x = 1.9$, 1.8, and 1.5 small amounts (∼1 wt %) of a binary iron nitride (FeN_x, $x \sim 0.5$) impurity were present in the product. The composition $Fe_{0.75}Ni_{1.25}Mo_3N$ was obtained pure and is the focus of measurements for this family of compounds. The products of the more Fe-rich compositions ($x = 1$, 0.75, 0.5) contained increasing amounts of impurities with the η-carbide structure observed for Fe_3Mo_3N, illustrating the preference of Fe for the η-carbide structure over the β-Mn structure. Clearly the composition of the β-Mn phase differs slightly from the ideal value in those samples which contain an impurity.

(21) Wells, A. F. *Three-dimensional nets and polyhedra*; Wiley: New York, 1977.
(22) Prior, T. J.; Nguyen-Manh, D.; Couper, V. J.; Battle, P. D. *J. Phys.: Condens. Matter* **2004**, *16*, 2273−2281.
(23) Rietveld, H. M. *J. Appl. Crystallogr.* **1969**, *2*, 65−71.
(24) Larson, A. C.; von-Dreele, R. B. *General Structure Analysis System* (GSAS), Report LAUR 86-748; Los Alamos National Laboratories: Los Alamos, NM, 1990.
(25) Rodriguez-Carvajal, J. *FULLPROF: A Program for Rietveld Refinement and Pattern Matching Analysis, Abstracts of the Satellite Meeting on Powder Diffraction of the XV Congress of the IUCr*, Toulouse, France, 1990; p 127.
(26) Roisnel, T.; Rodriguez-Carvajal, J. *Mater. Sci. Forum* **2001**, *378−381*, 118−123.

Table 1. Crystal Data for $Fe_{2-x}M_xMo_3N$ (M = Ni, Pd) Derived from X-ray Diffraction Data Collected at Room Temperature

		8c site (Fe/M)		12d site (Mo)		4a site (N)		
composition[a]	a_o/Å	x	U_{iso}/Å^2	y	U_{iso}/Å^2	U_{iso}/Å^2	impurity	R_{wp} (χ^2)
$Fe_{0.1}Ni_{1.9}Mo_3N$	6.63740(3)	0.0668(2)	0.0013(5)	0.20161(7)	0.0020(2)	0.003(3)	1.02(4)% Fe_2N	0.1166 (0.784)
$Fe_{0.2}Ni_{1.8}Mo_3N$	6.63918(5)	0.0671(2)	0	0.20180(8)	0	0	pure	0.1037 (0.935)
$Fe_{0.5}Ni_{1.5}Mo_3N$	6.64797(4)	0.0677(2)	0	0.20223(8)	0	0	pure	0.0807 (0.826)
$Fe_{0.75}Ni_{1.25}Mo_3N$	6.65673(5)	0.0679(1)	0.0171(6)	0.20242(8)	0.0169(4)	0.022(4)	pure	0.0652 (1.215)
$FeNiMo_3N$	6.66346(4)	0.0688(2)	0.0161(8)	0.2029(1)	0.0135(3)	0.025(6)	2.5(1)% Fe_3Mo_3N	0.0712 (1.083)
$Fe_{1.25}Ni_{0.75}Mo_3N$	6.67217(4)	0.0689(2)	0.0096(8)	0.2030(1)	0.0092(3)	0.0096(8)	5.7(1)% Fe_3Mo_3N	0.0658 (1.069)
$Fe_{1.5}Ni_{0.5}Mo_3N$	6.68077(4)	0.0694(3)	0.0079(9)	0.2033(1)	0.0111(3)	0.0079(9)	9.5(2)% Fe_3Mo_3N	0.0612 (1.171)
$Fe_{0.5}Pd_{1.5}Mo_3N$	6.79416(3)	0.0635(1)	0	0.2042(1)	0	0	pure	0.0998 (0.977)
$Fe_{0.75}Pd_{1.25}Mo_3N$	6.78010(5)	0.0648(2)	0.0104(6)	0.2045(2)	0.0083(4)	0	pure	0.1003 (1.058)
$FePdMo_3N$	6.76367(1)	0.0656(2)	0	0.2046(1)	0.0011(3)	0	pure	0.0720 (0.790)
$Fe_{1.25}Pd_{0.75}Mo_3N$	6.74792(6)	0.0666(2)	0.0088(7)	0.2046(2)	0.0081(5)	0	pure	0.1250 (1.722)
$Fe_{1.5}Pd_{0.5}Mo_3N$	6.72852(1)	0.0675(3)	0.0170(9)	0.2042(2)	0.0164(4)	0.016(7)	pure	0.0479 (1.045)
$Fe_{1.8}Pd_{0.2}Mo_3N$	6.7090(1)	0.0679(3)	0	0.2041(2)	0	0	9.2(1)% Fe_3Mo_3N	0.0586 (1.205)
$Fe_{1.9}Pd_{0.1}Mo_3N$	6.70554(5)	0.0686(3)	0	0.2039(2)	0.0020(4)	0	~17% Fe_3Mo_3N + Mo	0.0507 (1.092)
$Fe_{1.95}Pd_{0.05}Mo_3N$	6.70287(6)	0.0693(3)	0	0.2039(2)	0.0030(5)	0	~24% Fe_3Mo_3N + Mo	0.0520 (1.047)

[a] β-Mn structure M_2T_3X: space group $P4_132$; M (8c) x,x,x; T (12d) 1/8, y, 0.25 + y; X (4a) 3/8, 3/8, 3/8.

Table 2. Crystal Data for $Fe_{2-x}Pt_xMo_3N$ Derived from X-ray Diffraction Data Collected at Room Temperature

		8c site (Fe/Pt)			12d site (Mo/Pt)			4a site (N)		
composition[a]	a_o/Å	atom type (atom %)	x	U_{iso}/Å^2	atom type (atom %)	y	U_{iso}/Å^2	U_{iso}/Å^2	impurity	R_{wp}(χ^2)
$Fe_{0.5}Pt_{1.5}Mo_3N$	6.80440(6)	Fe (28.0(1)) Pt (72.0(1))	0.0663(1)	0.0040(4)	Mo (92.1(4)) Pt (7.9(4))	0.2039(2)	0.0058(5)	0	16.3(5)% Fe_2N + 1.4(1)% Pt_3Mo_2	0.1062 (1.381)
$Fe_{0.75}Pt_{1.25}Mo_3N$	6.78091(9)	Fe (41.1(2)) Pt (58.9(2))	0.0644(2)	0	Mo (93.6(3)) Pt (6.4(3))	0.20145(2)	0	0	0.43(7)% Mo	0.1092 (1.134)
$FePtMo_3N$	6.7623(2)	Fe (50) Pt (50)	0.0653(2)	0.0032(6)	Mo	0.2051(2)	0	0	2.75(8)% Mo	0.1001 (1.183)
$Fe_{1.25}Pt_{0.75}Mo_3N$	6.7513(1)	Fe (62.5) Pd (37.5)	0.0662(3)	0.0037(8)	Mo	0.2046(3)	0.0052(6)	0	pure	0.1119 (1.069)
$Fe_{1.5}Pt_{0.5}Mo_3N$	6.7348(1)	Fe (75) Pt (25)	0.0666(3)	0.0061(8)	Mo	0.2045(2)	0.0068(6)	0	pure	0.0819 (1.223)

[a] β-Mn structure M_2T_3X: space group $P4_132$; M (8c) x,x,x; T (12d) 1/8, y, 0.25 + y; X (4a) 3/8, 3/8, 3/8.

The introduction of Pd into the hypothetical compound Fe_2Mo_3N proved possible by reduction−nitridation. Five compositions in the series $Fe_{2-x}Pd_xMo_3N$ with $0.5 \leq x \leq 1.5$ were obtained in greater than 99.5% purity (x = 1.5, 1.25, 1.0, 0.75, 0.5). Analysis of X-ray diffraction data collected from these compounds showed that they too crystallize with the filled β-manganese structure with Fe and Pd disordered on the metal (10,3)-a network and the space in this network filled by Mo_6N octahedra (Table 1). Very small amounts (<1%) of molybdenum or Fe_3Mo_3N impurities were sometimes observed. There was no evidence in the X-ray diffraction patterns for ordering of the Fe and Pd within this network or for any substitution of Mo on the 12d sites in the Mo_6N octahedra by these elements. Consistent with the relative sizes of the metals, the unit cell parameter increased almost linearly with increasing Pd content. Chemical analysis of nitrogen content (Table 3) again showed full occupancy of the 4a interstitial site by nitrogen. It also proved possible to synthesize phases which were much richer in Fe, albeit in impure form. Compositions with x = 0.05, 0.1, and 0.2 yielded mixtures in which a compound with the filled β-manganese structure was dominant, although an impurity (~15%) with the η-carbide structure was also present.

Five compositions in this series $Fe_{2-x}Pt_xMo_3N$ (x = 1.5, 1.25, 1, 0.75, 0.5) were obtained by nitridation of metal oxides under reducing conditions. Analysis of X-ray diffraction data showed that a β-manganese phase is the dominant component in each product. $Fe_{1.5}Pt_{0.5}Mo_3N$ and $Fe_{1.25}Pt_{0.75}Mo_3N$ were obtained pure, compositions with x = 1 and 1.25 contained small amounts (~0.8%) of molybdenum metal, and $Fe_{0.5}Pt_{1.5}Mo_3N$ contained significant amounts (~18%) of FeN_x ($x \approx 0.5$) and an alloy with composition Pt_3Mo_2. Crystal data for the β-Mn phases are given in Table 2. Nitrogen analysis (Table 3) showed full occupancy of the 4a site. The refinement of structural models against X-ray diffraction data initially proceeded smoothly for these phases with Fe and Pt being disordered on the 8c site and Mo located on the 12d site. However, for the compositions x = 1.25 and 1.5, the fits, particularly at low angle, were rather poor. A much better fit (Figure 2) was obtained in both these cases when a small amount of Pt (ca. 5%) was introduced on the 12d site, consistent with the observation of a molybdenum impurity. The Fe:Pt ratio was

Table 3. Chemical Analysis Data for $Fe_{2-x}M_xMo_3N$

composition	calculated %N	observed %N (±0.02)
$Fe_{0.1}Ni_{1.9}Mo_3N$	3.34	3.46
$Fe_{0.2}Ni_{1.8}Mo_3N$	3.35	3.47
$Fe_{0.5}Ni_{1.5}Mo_3N$	3.35	3.52
$Fe_{0.75}Ni_{1.25}Mo_3N$	3.36	3.20
$FeNiMo_3N$	3.36	3.38
$Fe_{1.25}Ni_{0.75}Mo_3N$	3.37	3.34
$Fe_{1.5}Ni_{0.5}Mo_3N$	3.38	3.36
$Fe_{0.5}Pd_{1.5}Mo_3N$	2.86	2.98
$Fe_{0.75}Pd_{1.25}Mo_3N$	2.94	2.99
$FePdMo_3N$	3.01	3.01
$Fe_{1.25}Pd_{0.75}Mo_3N$	3.13	3.10
$Fe_{1.5}Pd_{0.5}Mo_3N$	3.19	3.25
$Fe_{0.5}Pt_{1.5}Mo_3N$	2.25	2.27
$Fe_{0.75}Pt_{1.25}Mo_3N$	2.38	2.38
$FePtMo_3N$	2.53	2.58
$Fe_{1.25}Pt_{0.75}Mo_3N$	2.70	2.75
$Fe_{1.5}Pt_{0.5}Mo_3N$	2.90	3.05

Table 4. Magnetic Properties of $Fe_{2-x}M_xMo_3N$ (M = Ni, Pd, Pt)

	M								
	Ni			Pd			Pt		
x	T_c/K	μ_{SAT}/μ_B per f.u.	μ_{SAT} per Fe	T_c/K	μ_{SAT}/μ_B per f.u.	μ_{SAT} per Fe	T_c/K	μ_{SAT}/μ_B per f.u.	μ_{SAT} per Fe
0.5	170	2.06(2)	1.37	160	2.44(2)	1.63	160	2.10(1)	1.40
0.75	180	1.82(2)	1.46	175	2.10(2)	1.68	225	2.10(2)	1.68
1	175	1.52(2)	1.52	160	1.73(2)	1.73	220	1.80(1)	1.80
1.25	150	1.10(2)	1.47	145	1.30(2)	1.73	200	1.46(2)	1.95
1.5	100	0.76(2)	1.52	110	0.83(1)	1.66	130	0.84(1)	1.68
1.8	15	0.25(2)	1.25						

maintained by increasing the concentration of Fe on the 8c site.

Magnetic Properties. SQUID magnetometry data collected for the $Fe_{2-x}Ni_xMo_3N$ compositions ($x = 1.8, 1.5, 1.25, 1, 0.75, 0.5$) suggested these were all ferromagnets at low temperature; magnetic data (μ_{SAT}, T_c) are given in Table 4. Measurements of magnetization as a function of field showed the samples all saturated in a field of approximately 1 T and displayed almost no hysteresis about the origin. Fe_3Mo_3N is a Pauli paramagnet[27] and the transitions observed for the impure samples having $0.5 \leq x \leq 1$ can therefore be attributed to the β-Mn phase. Magnetometry data for $Fe_{0.75}Ni_{1.25}Mo_3N$, which are typical of those collected from all compositions, are given in Figure 3. Neutron diffraction data were collected from $Fe_{0.75}Ni_{1.25}Mo_3N$ at 200 and 5 K using the instrument D1b. Analysis of data collected at 200 K affirmed the structure determined from the X-ray data and full occupancy by nitrogen of the 4a interstitial site. The data collected at 5 K showed additional Bragg scattering in the diffraction pattern, most notably in the 110 and 111 peaks, indicative of long-range magnetic order. This could be accounted for using a magnetic model with a ferromagnetic arrangement of spins on the 8c positions of the (10,3)-a net. The magnitude of the magnetic moment on each site was refined to 0.52(8) μ_B, which is in good agreement with the value of 0.55 μ_B per 8c site obtained from magnetometry.

SQUID magnetometry data for the four samples in the series $Fe_{2-x}Pd_xMo_3N$ with $0.5 \leq x \leq 1.5$ suggested these materials were also ferromagnetic at low temperature. Data are given in Table 4. Measurements as a function of field showed the samples all saturated in a field of approximately 1 T and displayed almost no hysteresis about the origin. Our previously[22] published neutron study of $Fe_{1.5}Pd_{0.5}Mo_3N$ affirmed the structure determined from the X-ray data, including full occupancy by nitrogen of the 4a interstitial site, and data collected at 5 K showed the presence of ferromagnetic order with a magnetic moment of 1.20(5) μ_B on each 8c site, in good agreement with the value of 1.22 μ_B obtained by magnetometry.

SQUID magnetometry data for compounds in the series $Fe_{2-x}Pt_xMo_3N$ are also given in Table 4. All the compounds were found to be ferromagnets with transition temperatures higher than the analogous Ni or Pd compounds. Once again, measurements of magnetization as a function of field showed very little hysteresis about the origin and showed that samples saturate in fields of 1 T. Neutron diffraction data were collected for the compositions $FePtMo_3N$ and $Fe_{0.75}Pt_{1.25}$-

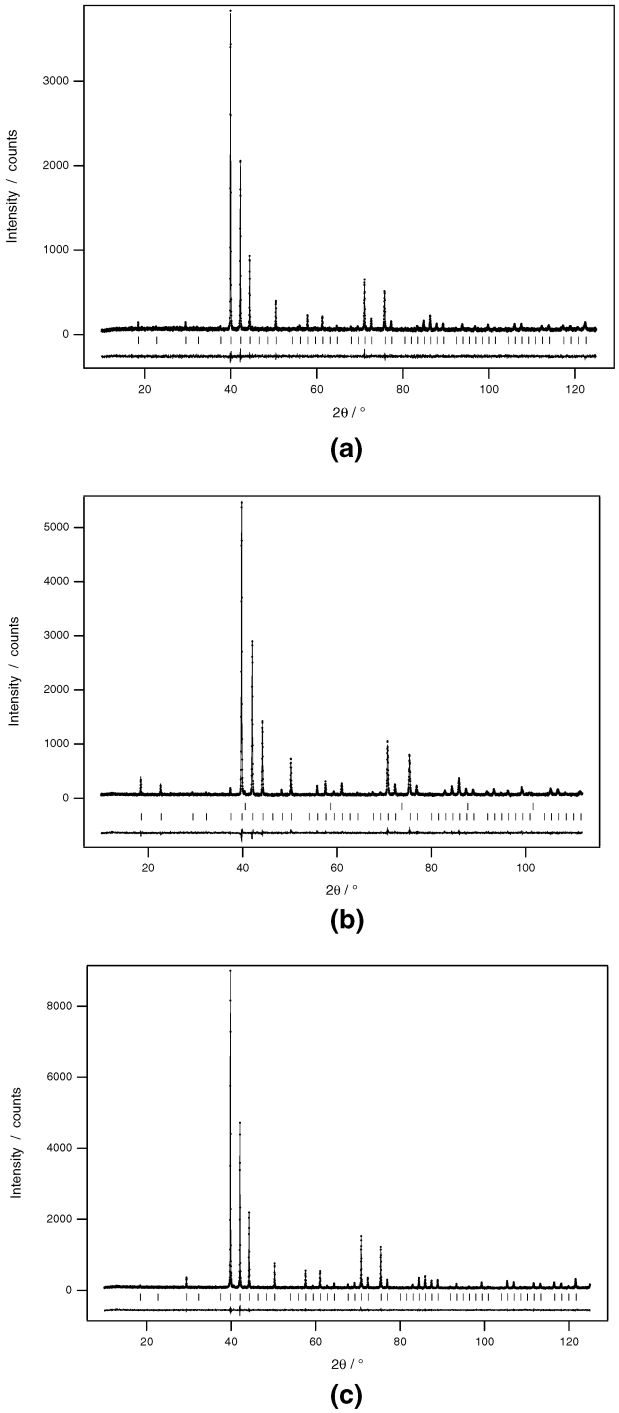

Figure 2. Observed (●), calculated (−), and difference X-ray powder diffraction profiles for (a) $Fe_{1.25}Pt_{0.75}Mo_3N$, (b) $Fe_{0.75}Pt_{1.25}Mo_3N$, with some Pt on the 12d site and a Mo impurity present, and (c) $Fe_{0.75}Pd_{1.25}Mo_3N$. The angular range $15 < 2\theta/° < 25$ is particularly sensitive to the metal distribution. Positions of allowed reflections are indicated by tick marks.

(27) Panda, R. N.; Gajbhiye, N. S. *J. Alloy Compd.* **1997**, *256*, 102−107.

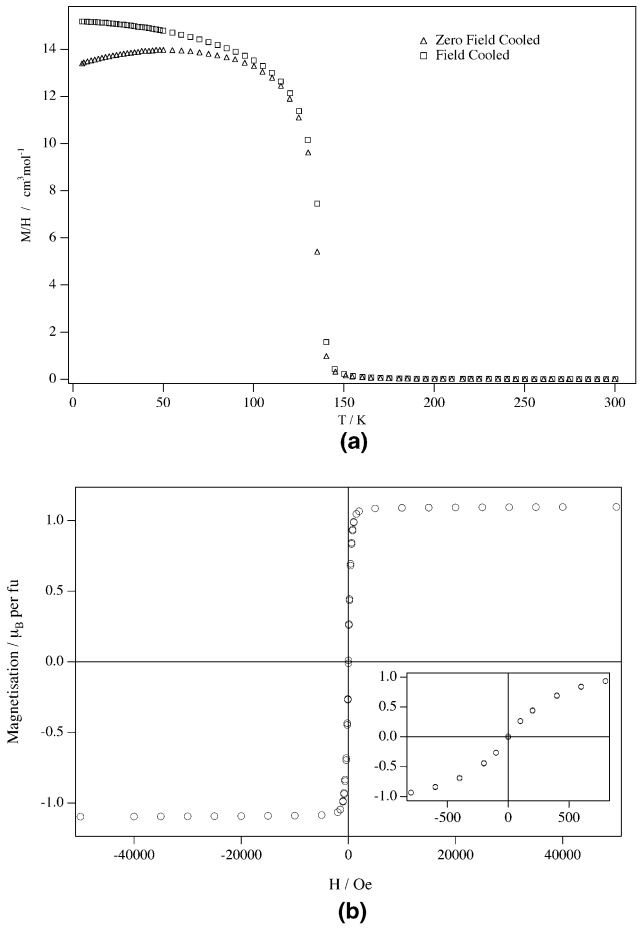

Figure 3. (a) Variation of molar magnetic susceptibility (M/H) with temperature of $Fe_{0.75}Ni_{1.25}Mo_3N$. (b) Magnetization of $Fe_{0.75}Ni_{1.25}Mo_3N$ as a function of applied field at 5 K. The inset shows the region around the origin expanded.

Mo_3N at 300 and 10 K using the instrument D2b. Analysis of the data collected at 300 K confirmed the structural features identified by X-ray diffraction, including full occupancy by nitrogen of the 4a position. The ratio of Pt to Mo on the 12d site in $Fe_{0.75}Pt_{1.25}Mo_3N$ was fixed at the value determined from the analysis of X-ray data because of the greater contrast in scattering lengths in this technique. Low-temperature data contained additional Bragg intensity at low angles which could be accounted for by a ferromagnetic arrangement of spins on the 8c site. The fit for $FePtMo_3N$ is displayed in Figure 4. The refined value of the moment on the 8c site was 1.05(3) and 0.91(6) μ_B for the $x = 1$ and 1.25 compositions, respectively; these values are somewhat higher than those of 0.9 and 0.73 μ_B obtained from magnetometry.

Electrical Conductivity. At 273 K all the samples studied display metallic behavior with a resistivity of the order 1×10^{-3} Ωcm as detailed in Table 5, and on cooling the resistivity of all samples intially falls. However, the behavior in the three series is not uniform and these materials can be classified into three basic types (A, B, and C) as illustrated in Figure 5. For $Fe_{2-x}M_xMo_3N$, when M = Ni, the compositions $x = 1$, 1.25, and 1.5 display metallic conductivity down to low temperatures (∼20 K), but with an increase in the gradient of $\rho(T)$ on cooling. This Type A behavior also occurs for $x = 0.5$ and $x = 0.75$ when M = Pd and $x = 0.5$ when M = Pt. For the remainder of the compositions, there is a change in the sign of $d\rho/dT$ on cooling. For Type B, M = Pt; $x = 1$ or 1.5, this negative gradient is then observed down to the lowest temperatures measured (Figure 5b), whereas for the remaining samples, Type C, M = Ni, $x = 1.8$; M = Pd, $x = 1$, 1.25, 1.5; M = Pt, $x = 0.75$ and 1.25 there is a return to a positive value of $d\rho/dT$ on further cooling (Figure 5c). However, although the behavior is never linear, the resistivity does not vary by more than ∼8% over the temperature range $30 < T/K < 273$.

Discussion

Iron displays some reluctance to enter the filled β-manganese structure if the alternative Fe_3Mo_3N (η-carbide) is available; reduction−nitridation of a 2:3 stoichiometric

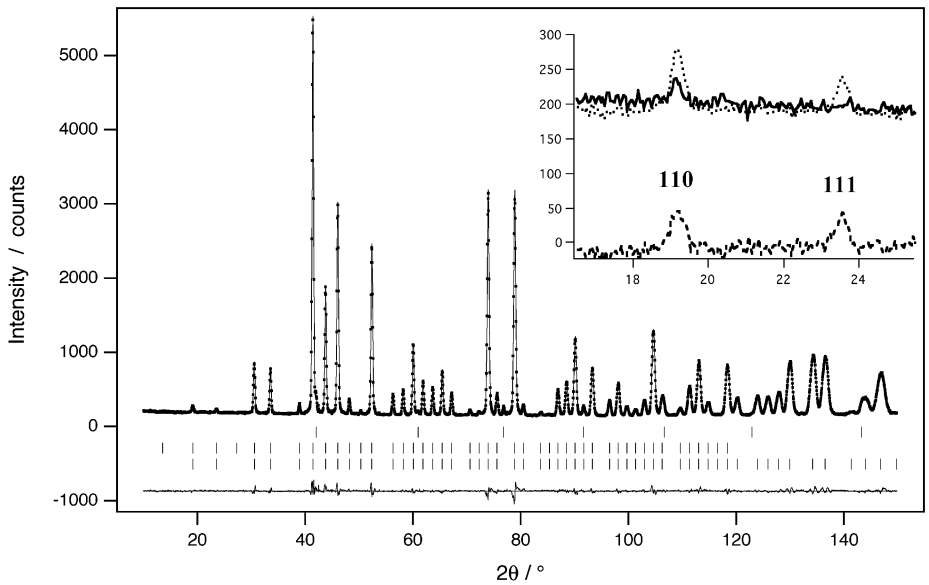

Figure 4. Observed (●), calculated (−), and difference neutron powder diffraction profiles for $FePtMo_3N$ at 10 K. The lower tick marks indicate positions of allowed structural reflections; the middle tick marks indicate allowed magnetic reflections; the upper set indicates positions of allowed reflections for the Mo impurity (2.8%). The inset shows data collected at 300 K (solid line), 10 K (dots), and their difference (lower, dashed line). Low-angle reflections which display additional intensity upon cooling below the Curie point are labeled with their Miller indices.

Table 5. Variation of Electrical Resistivity of $Fe_{2-x}M_xMo_3N$ (M = Ni, Pd, Pt) with Temperature and Composition

	M								
	Ni			Pd			Pt		
x	ρ/mΩcm at 273 K	behavior on cooling	T_1, T_2/K[a]	ρ/mΩcm at 273 K	behavior on cooling	T_1, T_2/K	ρ/mΩcm at 273 K	behavior on cooling	T_1, T_2/K
0.5	not studied (impure)			1.7	A	150	2.0	A	110
0.75	not studied (impure)			2.2	A	110	1.6	C	240,150
1	1.1	A	60	0.6	C	160, 100	1.2	B	200
1.25	0.9	A	100	1.7	C	200, 90	1.0	C	210, 50
1.5	0.9	A	70	1.6	C	220, 80	1.6	B	200
1.8	1.2	C	240, 70						

[a] T_1 and T_2 are defined for behavioral types A, B, and C in Figure 5.

mixture of Fe and Mo oxides does not lead to Fe_2Mo_3N, but to a mixture of composition $2Fe_3Mo_3N + 3Mo$. However, when accompanied by a group 10 metal on the (10,3)-a network, it is possible to obtain pure β-manganese phases which contain large amounts of Fe. It is remarkable that as little as 2.5% Pd in the reaction mixture leads to a product distribution dominated by a compound with the filled β-manganese structure and thus to a new family of ferromagnets.

Compounds in each series $Fe_{2-x}M_xMo_3N$ (M = Ni, Pd, Pt) adopt the filled β-manganese structure and the lattice parameter varies linearly as the metals are substituted for Fe (Figure 6). For the smaller Ni atom, the lattice parameter decreases, while for compounds containing Pd and Pt lattice parameters are almost identical in analogous compositions and increase with increasing group 10 metal content. Extrapolations of plots of the unit cell parameter against composition for these series allow estimation of a value 6.70(3) Å for the unit cell parameter of the hypothetical compound Fe_2Mo_3N.

It is very curious that, for compounds rich in Pt, it is possible to introduce Pt on to the 12d site, that is, to replace Mo in the network of Mo_6N octahedra. Although many groups have synthesized related filled β-manganese phases,[28−30] to our knowledge this is the first time it has been possible to substitute Mo on the 12d site. Mo and Pt display similar metallic radii no doubt as a consequence of the lanthanide contraction; this suggests other metals of similar radii may be incorporated in place of Mo.

All of the compounds described in this work are soft ferromagnets. For the Ni and Pd series the saturation magnetizaton varies linearly with Fe content in each case and band structure calculations have shown[22] that the moment in the phases is associated with the Fe atoms. However, T_c does not vary in a linear manner with Fe content for any of the series and in each case as the Fe content is varied a maximum value of T_c appears to be reached when $x \sim 0.75$. In the case of the Pt series the variation of magnetization with Fe content is not linear. Possible causes of the different magnetic behavior observed for M = Pt include the tendency

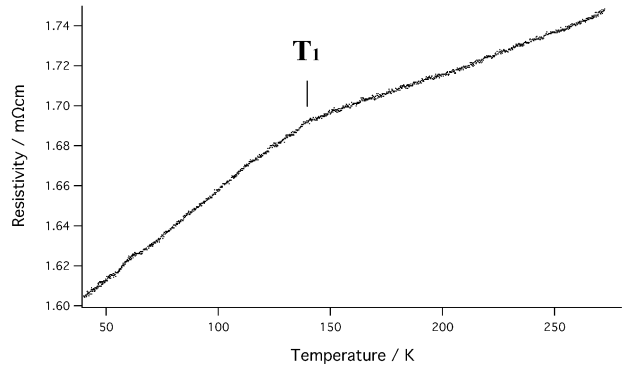

(a) TYPE A: $Fe_{1.5}Pd_{0.5}Mo_3N$

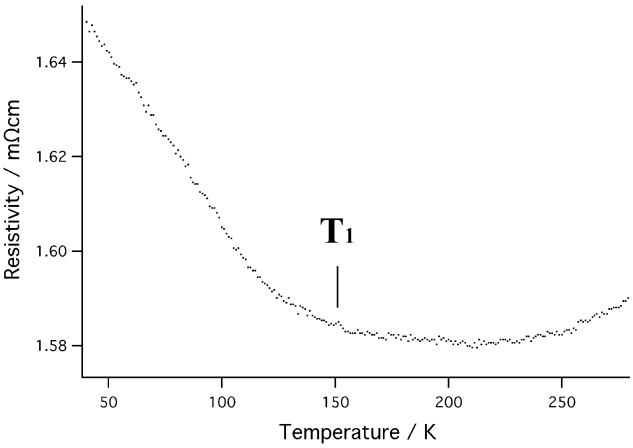

(b) TYPE B: $Fe_{0.5}Pt_{1.5}Mo_3N$

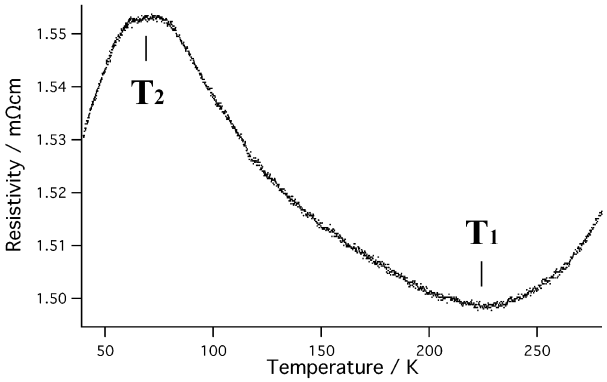

(c) TYPE C: $Fe_{0.5}Pd_{1.5}Mo_3N$

Figure 5. Variation of electrical resistivity with temperature for (a) $Fe_{1.5}Pd_{0.5}Mo_3N$, (b) $Fe_{0.5}Pt_{1.5}Mo_3N$, and (c) $Fe_{0.5}Pd_{1.5}Mo_3N$.

(28) El-Himri, A.; Sapina, F.; Ibanez, R.; Beltran, A. *J. Mater. Chem.* **2001**, *11*, 2311−2314.
(29) Herle, P. S.; Hegde, M. S.; Sooryanarayana, K.; Row, T. N. G.; Subbanna, G. N. *Inorg. Chem.* **1998**, *37*, 4128−4130.
(30) Herle, P. S.; Hegde, M. S.; Sooryanarayana, K.; Row, T. N. G.; Subbanna, G. N. *J. Mater. Chem.* **1998**, *8*, 1435−1440.

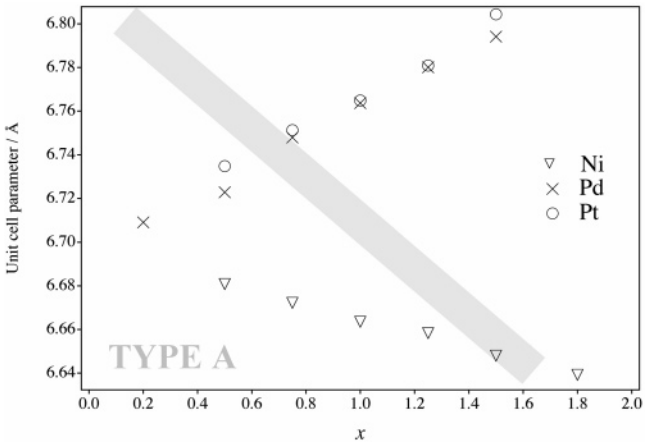

Figure 6. Composition dependence of the unit cell parameter of $Fe_{2-x}M_xMo_3N$ (M = Ni, Pd, Pt). Compositions below the shaded band all show Type A variation of resistivity with temperature.

of this element to occupy the 12d site. Spin-polarized band structure calculations are needed to elucidate this point, but the analogous calculations for M = Pd show that the 12d site contributes states at the Fermi level, and any change in the electron density at this site is therefore likely to modify the electronic behavior, both magnetic and electrical. The growing importance of spin−orbit coupling on descending the group might also lead to the observation of different behavior for M = Pt.

A wide range of electrical behavior is observed across the range of compositions studied. Our band structure calculations for M = Pd[22] show that the Fermi level is composed of Fe-derived states from the 8c sites and Mo-derived states from the 12d sites; the Pd-derived states lie well below the Fermi level. The Ni-derived states will lie considerably higher in energy than those from Pd (3d vs 4d orbitals), and although centered lower than those from Fe, they might contribute at the Fermi level, thus causing all but the most Fe-deficient composition measured ($x = 1.8$) to show metallic, type A character over the accessible temperature range. This behavior is only observed in the most Fe-rich of our Pd and Pt-containing samples, consistent with the idea that the introduction of 4d and 5d metal orbitals removes states from the Fermi level. The dominance of Type-A behavior in iron-rich compositions and those with low unit cell volumes is emphasized in Figure 6. On the basis of the data currently available, we are unable to offer a detailed explanation for the low-temperature behavior (Type B and Type C) of the Pd or Pt-containing samples, although we expect that the origin of the orbitals involved, variations in the occupancy of the 12d site, the number of electrons in the system, and the unit cell parameter will all play a role in determining the density of states at the Fermi level and hence the conductivity. Further studies, both experimental and computational, are planned in order to elucidate this point. Nevertheless, it is clear from the data presently available that the use of a surprisingly simple synthetic method has led to the discovery of a new and extensive family of metallic ferromagnets, albeit with Curie temperatures below room temperature. Raising the magnetic ordering temperature is one of the immediate goals of our program in this area.

Acknowledgment. We are grateful to EPSRC for financial support, to E. Suard and T. Hansen for experimental assistance at ILL, Grenoble, and to D. Nguyen-Manh for helpful discussions.

Supporting Information Available: Table S1 listing structural parameters of $Fe_{2-x}M_xMo_3N$ (M = Ni, Pd, Pt) refined from neutron diffraction data (PDF). This material is available free of charge via the Internet at http://pubs.acs.org.

CM047859Q